Enhanced Fermi-Surface Nesting in Superconducting $BaFe_2(As_{1-x}P_x)_2$ Revealed by the de Haas–van Alphen Effect

J. G. Analytis,[1,2] J.-H. Chu,[1,2] R. D. McDonald,[3] S. C. Riggs,[1,2] and I. R. Fisher[1,2]

[1]*Stanford Institute for Materials and Energy Sciences, SLAC National Accelerator Laboratory, 2575 Sand Hill Road, Menlo Park, California 94025, USA*

[2]*Geballe Laboratory for Advanced Materials and Department of Applied Physics, Stanford University, Stanford, California 94305, USA*

[3]*Los Alamos National Laboratory, Los Alamos, New Mexico 87545, USA*

(Received 5 February 2010; published 12 November 2010)

The three-dimensional Fermi-surface morphology of superconducting $BaFe_2(As_{0.37}P_{0.63})_2$ with $T_c = 9$ K is determined using the de Haas–van Alphen effect. The inner electron pocket has a similar area and k_z interplane warping to the observed hole pocket, revealing that the Fermi surfaces are geometrically well nested in the (π, π) direction. These results are in stark contrast to the fermiology of the nonsuperconducting phosphides ($x = 1$), and therefore suggest an important role for nesting in pnictide superconductivity.

DOI: 10.1103/PhysRevLett.105.207004 PACS numbers: 74.25.Jb, 71.18.+y, 74.20.Pq, 74.25.Bt

A common ingredient in theories of high-temperature superconductivity is the role of Fermi-surface (FS) nesting—a property originating from the shape of the FS which enhances quasiparticle scattering along particular directions in momentum space. FSs that support nesting are typically low dimensional with a weakly varying morphology in at least one direction in momentum space. In the case of the Fe pnictides, it is nesting in the (π, π) direction between electron and hole FSs which is most often invoked [1–6]. From the earliest band structure calculations on the ''1111'' compounds, e.g., LaFeAsO, it was clear that this was a possible mechanism to explain both the magnetism and the superconductivity [6]. However, the ''122'' parent pnictides, e.g., $BaFe_2As_2$, do not have such a strongly nested FS, yet have comparable Néel temperatures and similar magnitudes for the ordered moments [4]. Furthermore, LaFePO has a FS which is measured to have well-matched electron and hole pockets, and is therefore close to satisfying a nesting condition, yet has no known magnetic ordering [7,8]. This has led several authors to invoke the local environment, particularly of the As-Fe-As bond angle and bond length, as a route to understanding these cases [3,4,9]. The role of nesting in this family of compounds is therefore highly debated. In order to determine whether a given FS supports nesting, an intimate knowledge of the full three-dimensional morphology is required, and this is the purpose of the present study.

We investigate single crystals of superconducting $BaFe_2(As_{0.37}P_{0.63})_2$, $T_c = 9$ K. The compounds $BaFe_2As_2$ and $BaFe_2P_2$ are nominally isoelectronic since P and As have the same number of valence electrons. The former orders antiferromagnetically at ~138 K, whereas the latter is an ordinary metal down to the lowest temperatures measured. For intermediate compositions there is a superconducting dome that peaks at $x \sim 0.3$, with $T_c = 30$ K. These materials are particularly useful for de Haas–van Alphen (dHvA) studies because the disorder is weak and long mean-free paths can be maintained. As a consequence, quantum oscillatory phenomena can be measured, as demonstrated recently by Shishido *et al.* [10]. This earlier work revealed two important observations: first, the size of the FS increases with x beyond optimal As/P substitution, and second, the effective mass decreases. However, due to the resolution limits of the data the details of the three-dimensional curvature of the FS could not be determined for the superconducting compounds and no hole pockets were observed. In this Letter we resolve the morphology of the electron pockets and that of one hole pocket. We conclude that a large amount of the FS is geometrically nested. The details revealed in this study provide compelling evidence that nesting plays a key role in the superconducting mechanism in this family of compounds.

High quality single crystals of $BaFe_2(As_{1-x}P_x)_2$ with in-plane residual resistivity ratios $\rho(300\ \mathrm{K})/\rho(1.8\ \mathrm{K}) \sim 20$ were grown from an FeAs flux (see supplementary material [11]). The composition $x = 0.63(3)$ was determined by microprobe analysis. Torque magnetometry was performed using piezoresistive microcantilevers in fields of up to 35 T in dc Bitter magnets at the NHMFL, Florida. The oscillatory part of the torque signal $\mathbf{T} \propto \mathbf{M} \times \mathbf{B}$ originates from the dHvA effect. Each dHvA frequency is related to an extremal cross-sectional area A_k of the FS in momentum space via the Onsager relation $F = (\hbar/2\pi e)A_k$. For simply warped, quasi-two-dimensional cylinders two frequencies are expected, a maximum (''belly'' orbit) and a minimum (''neck'' orbit). As the angle of the field with respect to the sample is changed, these extremal orbits traverse larger sections of the FS, and at Yamaji angles, all cross-sectional orbits match, enhancing the oscillatory amplitude [12]. Band structure calculations were performed for the end

members $BaFe_2As_2$ and $BaFe_2P_2$ using an augmented plane wave plus local orbital method as implemented in the WIEN2K code [11,13]. The composition $x = 0.63$ does not have a structural transition at low temperature and therefore the (room temperature) experimentally determined tetragonal unit cell parameters are used. These are $a = 3.96(3.84)$ Å, $c = 13.039(12.44)$ Å and $z_P = 0.3538(0.3456)$ for the As(P) variants.

dHvA oscillations are observed in the torque signal for fields above ~20 T. In Figs. 1(a)–1(c) we show the background subtracted data at three typical angles. The Fourier spectrum is generated by implementing discrete Fourier transform methods on the signal (in inverse field) for each angle and is shown in adjacent panels. At most angles the spectrum is dominated by two (split) peaks which we label $\alpha_{1,2}$ and $\beta_{1,2}$. In total five frequencies are observed, which we denote as α_1, α_2, β_1, β_2, and γ. We observe a further low frequency labeled ϵ, which has some scatter about a value of 250 T at most angles. However, its value is sensitive to the background subtraction and the field window used and so is not included in the remaining analysis. In both LaFePO [7] and $SrFe_2P_2$ [14] the strongest signal was from the electron pockets, which tend to have the longest mean-free paths. It is natural to assume that this remains the case in the doped compounds, and we therefore assign the α and β frequencies to the electron pockets, suggesting the third frequency γ is most likely a hole pocket.

The calculated FS for $BaFe_2P_2$ and $BaFe_2As_2$ (in the tetragonal structure) is shown in Figs. 2(b) and 2(c), respectively. Both consist of two similarly warped concentric electron cylinders at the X point. $BaFe_2As_2$ consists of three hole sheets while $BaFe_2P_2$ consists of only two hole pockets centered at the Γ point. The hole sheets of $BaFe_2P_2$ are much more warped than $BaFe_2As_2$, consistent with dHvA measurements on $SrFe_2P_2$ [14], suggesting $BaFe_2As_2$ is closer to satisfying a nesting condition. The calculated dHvA angle dependence associated with these FSs for $BaFe_2P_2$ and $BaFe_2As_2$ can be found in Ref. [11], where we also include rigid-band shifts to account for the structure seen in the data.

All the dHvA frequencies expected from the band structure of $BaFe_2As_2$ and $BaFe_2P_2$ deviate substantially from our observations [11]. The discrepancy between the experimentally determined FS cross sections and those calculated for the end members ($x = 0$ and 1) cannot be reconciled by using the experimentally determined lattice parameters for the $x = 0.63$ compound, which only weakly affect the calculation. However, moderate rigid-band shifts can fit the data as shown in Ref. [11], with the following caveats. First, even with the best fit rigid-band shifts to the band structure of $BaFe_2As_2$ or $BaFe_2P_2$ we observe significantly less k_z warping than can be reproduced by the calculation for the α and γ pockets. Second, the Yamaji angle of the γ pocket deviates by about 15° from the data. However, fitting the γ frequency to a simple (cosine) warped cylinder, much better agreement is achieved with the experimental data and the Yamaji angle at ~51° is almost perfectly matched, as shown in Fig. 2(a). The experimentally determined FS can support nesting much more strongly than predicted by the calculated band structure (or indeed the experimentally determined FS [14,15]) of the end members.

Plotting $F\cos\theta$ versus angle [Fig. 2(a)] reveals that β_1 and β_2 are neck and belly frequencies of a single pocket with moderate warping. Similarly, the α_1 and α_2 are likely neck and belly frequencies of a single pocket with comparable warping. This assignment is consistent with their

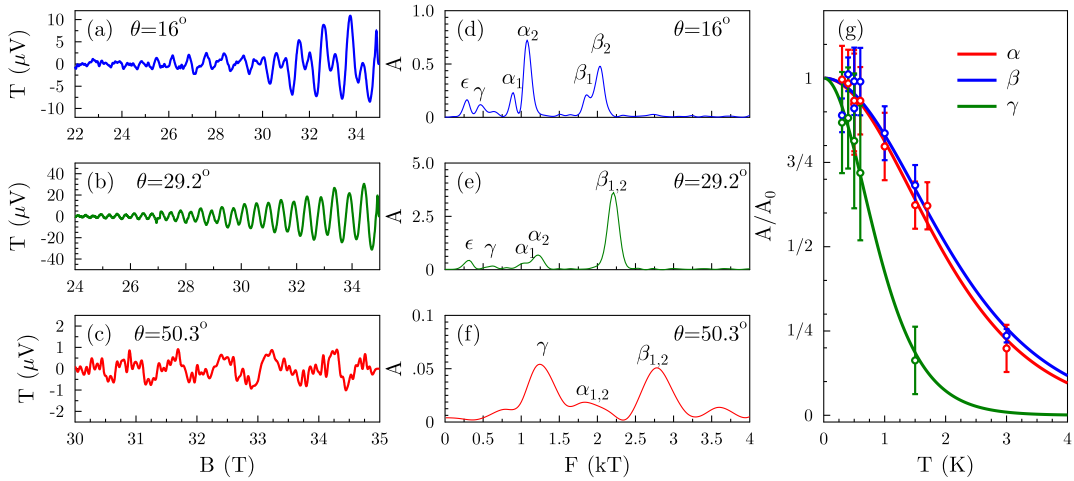

FIG. 1 (color online). The background subtracted raw data (a)–(c) for three different angles taken at $T = 0.3$ K, and corresponding Fourier spectra in (d)–(f). The Fourier amplitudes of (e) and (f) are normalized with respect to (d) for clarity. The γ pockets have an enhanced amplitude near $\theta \approx 51°$ probably due to a Yamaji effect. Panel (g) gives the Fourier amplitude as a function of temperature with Lifshitz-Kosevich fits for the β (blue line), α (red line), and γ (green line) pockets, from which we determine the effective mass. Data for (g) were taken at $\theta = 16°$. Raw data for the above are given in the supplemental material [11], in addition to fast Fourier transforms from all other angles.

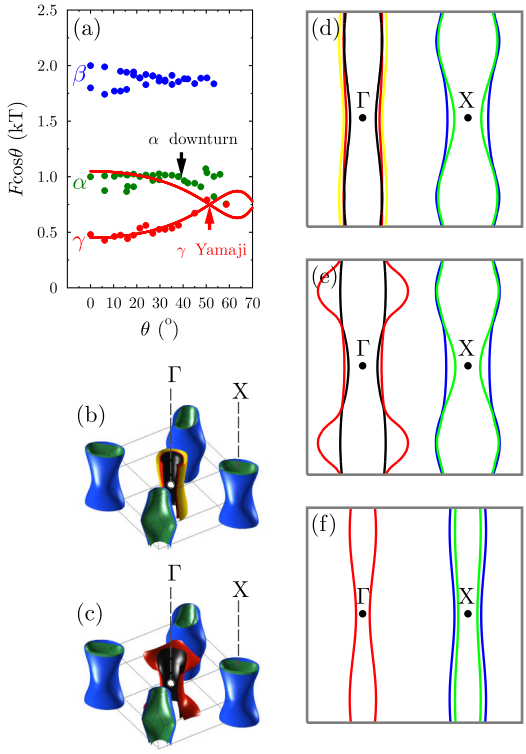

FIG. 2 (color online). (a) The observed dHvA frequencies plotted as $F\cos\theta$ (see also supplementary material [11]). The observed downturn in the α pocket joining the Yamaji angle of the γ pocket is shown. Panels (b) and (c) show the FS as calculated for $BaFe_2As_2$ and $BaFe_2P_2$, respectively. The hole pockets are centered at the Γ point (marked by a white dot) of the Brillouin zone and the electron pockets at the X points (hidden inside the electron pocket). Two-dimensional sections through the FS in the (110) plane shown for unshifted band structures in (d) for $BaFe_2As_2$ and (e) for $BaFe_2P_2$. In (f) we show the electron pockets after shifting the $BaFe_2As_2$ bands to agree with our dHvA measurements, and the fitted cosine warped cylinder is shown for the hole pocket.

similar effective mass (see Table I). The high angle data are vital for the assignment of the γ pocket. Approaching 50° the α frequency (scaled by $\cos\theta$) abruptly turns down [see arrow in Fig. 2(a)], only to appear again near its average value at still higher angles. Simultaneously, the γ frequency turns upward, joining the α downturn at around 51°. This suggests that for much of the angular range the α spectrum in fact contains a third frequency, the belly of the γ pocket. Furthermore, at 51° the spectrum of the amplitude of the γ is enhanced beyond that of the α frequency, indicating the first Yamaji angle for this pocket [see Fig. 1(f)]. We can gain an estimate of the interlayer transfer integral $t_\perp$ by approximating the warping as a simple cosine. Though such warping does not satisfy the correct symmetry constraints of the Brillouin zone, we nevertheless estimate $t_\perp = \hbar e/m^*(F_{\max} - F_0)$, where F_0 is frequency associated with the average Fermi wave vector [12], as shown in Table I. While it is possible that the γ orbit originates from the same FS as the α orbit, this seems unlikely given firstly that the α orbit remains at the average value of ~950 T at angles >51° and the effective mass of γ is around twice that of α (see below). We conclude that γ is a hole pocket. Even without further analysis, it is clear that this compound has at least one hole pocket which is geometrically well matched to the inner electron pocket.

The dHvA mean-free path and effective mass are extracted in the conventional manner using the Lifshitz-Kosevich formula [16] and the results are summarized in Table I. The data which entered the analysis are shown in Fig. 1(g). As expected, the hole pocket has a significantly shorter mean-free path than the electron pockets. For the effective mass, the α and β pockets are in good agreement with those reported in Ref. [10]. The effective mass of γ has the largest error bar because of the spectral leakage from low frequency noise in the Fourier spectrum, which tends to enhance the mass. Nevertheless, it is clear that the effective mass is around twice that of the electron pockets. In order to determine the renormalization we compare our masses to that of the shifted band structure of $BaFe_2As_2$ in Table I. We could have equally chosen to compare to $BaFe_2P_2$, in which case the renormalization would be roughly double that shown in the table. The mass enhancements are different for electron and hole pockets, being about $\lambda = m^*/m_b - 1 \sim 0.8$ for the α and β pockets and $\lambda = m^*/m_b - 1 \sim 2.6$ for the γ orbit. These enhancements are much larger than expected from electron-phonon coupling alone ($\lambda_{e\text{-ph}} \simeq 0.25$) [17]. Interestingly, the

TABLE I. Measured dHvA frequencies, effective masses (m^*), and mean-free paths (ℓ), along with the values from the band structure calculations. The experimental masses were determined at $\theta = 16°$. The band structure values are also estimated at the same angle from band structure calculations. Mean-free paths could not be calculated separately for both neck and belly orbits due to limits in the data resolution.

	Experiment			Calculations				
	F (kT)	$\frac{m^*}{m_e}$	ℓ (nm)	Orbit	F (kT)	$\frac{m_b}{m_e}$	$\frac{m^*}{m_b}$	$t_\perp$ (meV)
γ	0.45	4.5(5)	12	$2_{\min}$	0.53	1.24	3.6	8
				$2_{\max}$	0.86	1.72		
α_1	0.89	2.3(1)	⋯	$5_{\min}$	1.02	1.25	1.8	5
α_2	1.10	2.10(5)	48	$5_{\max}$	1.04	1.31	1.6	
β_1	1.80	2.1(1)	⋯	$4_{\min}$	1.81	1.17	1.8	7
β_2	2.01	2.0(5)	57	$4_{\max}$	1.95	1.30	1.5	

nonsuperconducting compounds have electron pockets with a greater enhancement than the holes, in contrast to the present case [14]. This study illustrates that as the superconducting dome is entered this electron-hole mass enhancement asymmetry is reversed, suggesting a vital role for many-body effects.

The total electron count from α and β is 0.1 electrons per unit cell, whereas the γ pocket accounts for only 0.03 holes per unit cell (approximately equivalent to the α electron pocket), leaving 0.07 uncompensated holes. As such one further hole pocket must exist that is not presently observed. Intriguingly, the contributions of the α and γ pocket almost perfectly compensate each other, and so the remaining FS must compensate the β pocket. This suggests the possibility that the remaining FS is of a similar size to the β pocket, which may therefore sustain FS nesting between the two outer electron or hole pockets, in addition to the inner.

The nature of the dimensionality of the electron and hole FSs and the consequent nesting has been extensively debated in the literature. Recently, the importance of dispersion in k_z has been illustrated in a number of photoemission studies, particularly on Co-doped compounds [18–21]. Some of these studies [18,20,21] emphasize two-dimensionality and (π, π) nesting for the undoped compounds, possibly explaining the spin density wave (SDW) formation, but suggest that doping electrons increases the dimensionality and suppresses the nesting, leading to superconductivity. In contrast, other studies [19,22,23] have suggested that nesting may play a very small role in the formation of the SDW in the undoped compounds, but under doping conditions where electron and hole pockets are of similar sizes, superconductivity is favored. However, as pointed out by Brouet *et al.* [19] it is vital to establish the dispersion in k_z in order to prove this, which we unambiguously do in the present study.

dHvA studies of the nonsuperconducting "122" arsenides ($x = 0$) reveal a FS which is consistent with a reconstruction from a moderately warped FS, as shown in Fig. 2(a) [15]. The phosphides reveal an unreconstructed FS which is far from satisfying a nesting condition, largely consistent with band structure calculations as shown in Fig. 2(b) [14]. In stark contrast, the present work shows that the intermediate superconducting compositions have very well matched electron and hole FSs as shown in Fig. 2(c), and therefore satisfy nesting better than either end member, yet there is no density wave reconstruction. This indicates that the nesting interaction is more relevant to the particle-particle (superconducting pairing) channel than the particle-hole (density wave nesting) channel. Furthermore, the superconducting compounds have significantly smaller FSs than expected by band structure, in line with interband scattering theory of Ortenzi *et al.* between well-nested Fermi surfaces [24]. This observation also appears consistent with several photoemission studies on both electron and hole doped compounds [19,20,22,23]. At smaller values of x with a higher T_c it is likely that this trend continues and the hole pockets even more closely match the electron pockets, becoming ever more difficult to observe in dHvA studies and perhaps explaining their absence in the data of Ref. [10].

The authors would like to thank Antony Carrington for useful comments and E. A. Yelland for access to computer software. R. D. M. acknowledges support from the BES "Science in 100 T" program. The NHMFL is supported by the NSF Division of Materials Research through DMR-0654118 and the State of Florida. J. G. A., J. H. C., and I. R. F. acknowledge support by the U.S. DOE, Office of Basic Energy Sciences under Contract No. DE-AC02-76SF00515.

[1] V. Cvetkovic and Z. Tesanovic, Europhys. Lett. **85**, 37002 (2009).
[2] A. V. Chubukov, D. V. Efremov, and I. Eremin, Phys. Rev. B **78**, 134512 (2008).
[3] K. Kuroki, H. Usui, S. Onari, R. Arita, and H. Aoki, Phys. Rev. B **79**, 224511 (2009).
[4] I. Mazin and J. Schmalian, Physica (Amsterdam) **469C**, 614 (2009).
[5] T. A. Maier, S. Graser, D. J. Scalapino, and P. J. Hirschfeld, Phys. Rev. B **79**, 224510 (2009).
[6] D. J. Singh and M. H. Du, Phys. Rev. Lett. **100**, 237003 (2008).
[7] A. I. Coldea *et al.*, Phys. Rev. Lett. **101**, 216402 (2008).
[8] D. H. Lu *et al.*, Nature (London) **455**, 81 (2008).
[9] T. Yildirim, Phys. Rev. Lett. **101**, 057010 (2008).
[10] H. Shishido *et al.*, Phys. Rev. Lett. **104**, 057008 (2010).
[11] See supplementary material at http://link.aps.org/supplemental/10.1103/PhysRevLett.105.207004 for details about band structure calculations and best fits to the data.
[12] K. Yamaji, J. Phys. Soc. Jpn. **58**, 1520 (1989).
[13] P. Blaha, K. Schwarz, G. K. H. Madsen, D. Kvasnicka, and J. Luitz, WIEN2K, edited by Karlheinz Schwarz, Technische Universität Wien, Austria, 2001.
[14] J. G. Analytis *et al.*, Phys. Rev. Lett. **103**, 076401 (2009).
[15] J. G. Analytis *et al.*, Phys. Rev. B **80**, 064507 (2009).
[16] D. Shoenberg, *Magnetic Oscillations in Metals* (Cambridge University Press, Cambridge, England, 2009), 1st ed.
[17] L. Boeri, O. V. Dolgov, and A. A. Golubov, Phys. Rev. Lett. **101**, 026403 (2008).
[18] P. Vilmercati *et al.*, Phys. Rev. B **79**, 220503 (2009).
[19] V. Brouet *et al.*, Phys. Rev. B **80**, 165115 (2009).
[20] S. Thirupathaiah *et al.*, Phys. Rev. B **81**, 104512 (2010).
[21] C. Liu *et al.*, Phys. Rev. Lett. **102**, 167004 (2009).
[22] K. Terashima *et al.*, Proc. Natl. Acad. Sci. U.S.A. **106**, 7330 (2009).
[23] T. Sato *et al.*, Phys. Rev. Lett. **103**, 047002 (2009).
[24] L. Ortenzi, E. Cappelluti, L. Benfatto, and L. Pietronero, Phys. Rev. Lett. **103**, 046404 (2009).